https://doi.org/10.5194/egusphere-2026-2396
Preprint. Discussion started: 20 May 2026

Marine Stratocumulus to Land Fog Transition in the Coastal Mountain-Range of Atacama Desert

Lobos-Roco Felipe[1,2], Espinoza Vicente[1,4], Keim-Vera Klaus[1,5], Muñoz Francisca[2], Suárez Francisco[1,3], and Hartogensis Oscar[4]

[1]Centro UC Desierto de Atacama, Pontificia Universidad Católica de Chile, Santiago, Chile
[2]Facultad de Agronomía y Sistemas Naturales, Pontificia Universidad Católica de Chile, Santiago, Chile
[3]Departamento de Ingeniería Hidráulica y Ambiental, Pontificia Universidad Católica de Chile, Santiago, Chile
[4]Meteorology and Air Quality group, Wageningen University, Wageningen, The Netherlands
[5]Institute of Meteorology and Climate Research, Karlsruhe Institute of Technology (KIT), Karlsruhe, Germany

Correspondence: Lobos-Roco Felipe (flobosr@uc.cl)

Abstract.

The advection of marine stratocumulus clouds (Sc) from the Southeast Pacific into the Atacama Desert forms extensive, semi-permanent fog banks at the top of the coastal mountain range. These fog banks provide the sole water input for xeric ecosystems and serve as a freshwater resource for human activities. To improve our understanding of this relevant system, we conducted a field experiment in July 2024 at the coastal Atacama called *StraToFog* to measure vertical profiles and near-surface parameters related to the marine boundary layer (MBL) state during the marine Sc-to-land fog transition. In this study, we aim to describe the campaign and present some of the first results from observations of the main processes at non-local and local scales during the Sc-fog transition. The vertical profile measurements reveal that the cloud-topped MBL frequently reaches 15 km inland, with negligible thermal changes but a significant decrease in humidity, suggesting fog and water vapour retention on the coastal mountains. We found that maximum fog collection occurs in the afternoon, driven by a sea-to-land breeze that transports higher marine humidity, thereby increasing liquid water content. During the night, fog collection decreases due to lower wind speed and liquid water content resulting from lower air temperature. At the surface, our observations suggest that negative latent heat flux is produced by dewfall at dawn, water vapour adsorption during midday, and fog deposition over the afternoon. The *StraToFog* field experiment revealed key acting processes, linking spatial scales to understand atmospheric water pathways in this hyperarid environment.

1 Introduction

The regular advection of the marine stratocumulus (Sc) from the Southeast Pacific Ocean into the western margin of South America between 18° S and 35° S results in fog at the coastal mountain range of Chile (Espinoza et al., 2024). This process transports a significant amount of humidity to the driest place on Earth: the Atacama Desert (del Río et al., 2018; Lobos-Roco et al., 2018; García et al., 2021). The main physical mechanism controlling ocean-to-desert Sc advection is the diurnal sea-land breeze (Rutllant et al., 2013). This breeze brings saturated air and significant amounts of water vapor, into contact with the

https://doi.org/10.5194/egusphere-2026-2396
Preprint. Discussion started: 20 May 2026

hyperarid coastal mountains of the Atacama Desert, producing fog and dewfall (Lobos-Roco et al., 2024). Fog represent the sole source of water in ecosystems composed of biological soil crusts, shrubs, and herbs adapted to extreme dry conditions (Muñoz-Schick et al., 2001). These ecosystems exhibit high endemism due to the localized heterogeneous patches where fog interacts with the complex topography (Pinto et al., 2006). Moreover, these water inputs represent a complementary water source that is currently harvested for human consumption, specifically for basic domestic activities (Schemenauer and Cereceda, 1994; Larrain et al., 2002) and agriculture (Albornoz et al., 2023). Due to ecological and social importance of fog in the Atacama, more attention is being given to the surface-atmospheric processes behind fog formation in the region. Here, the transition zone between the marine Sc over the Pacific to land fog in the Atacama is key because it involves different physical processes across non-local and local scales that are not yet fully understood.

At the synoptic scale, Sc clouds cover an enormous ($\sim$23%) area over the Pacific Ocean, affecting the Earth's radiation balance (Wood, 2012). The main physical process involved in the Sc cloud topped marine boundary layer (MBL) formation and maintenance is the thermal inversion (Espinoza et al., 2024). This inversion results from the contrast between the cool air of the MBL and the warm air of the free troposphere. While sea surface temperature (SST) cools the MBL (Thiel et al., 2007), the downward branch of the Hadley cell heats adiabatically the free troposphere through subsidence (Rutllant et al., 2013). This well-formed thermal inversion acts as a physical barrier, impeding the mixing of cool-humid air with hot-dry air aloft, resulting in the condensation of the cool and humid air in an extensive and continuous Sc cloud within the MBL $\sim$1000 m ASL (Rahn and Garreaud, 2010). These clouds are dominated by turbulent motions driven by air downdrafts resulting from radiative longwave cooling at the cloud top (CT), which not only entrains dry air into the MBL but also enhances the MBL cooling. The marine Sc presents a well-defined liquid water content structure, which increases almost linearly from the cloud base (CB) to the CT (Duynkerke et al., 1996; Wood, 2012).

From a local perspective, the Sc cloud deck formed over the ocean is advected several kilometres inland by the diurnal sea-land breeze, a thermally-driven wind between the cool ocean and a hot desert (Rutllant et al., 2003; Lobos-Roco et al., 2021). During this transition, the Sc cloud deck is intercepted by coastal hyperarid mountains whose peaks summits range from 500 to 1500 m ASL (Lobos-Roco et al., 2024), forming local fog banks (del Río et al., 2018) typically localized between 600 and 1200 m ASL, with a vertical thickness of $\sim$200 m (Del Río et al., 2021). Furthermore, topographic irregularities shape how much the Sc penetrates inland (Keim-Vera et al., 2024), while the spatial distribution of fog interception is further conditioned by the orientation of the mountain slopes (Lobos-Roco et al., 2025). On these mountains, fog can be intercepted by rocks, sparse vegetation, and artificial collectors (Schemenauer and Cereceda, 1994), whose small surface area can collect a significant amount of water. Despite the extensive efforts to understand marine land fog in the Atacama at non-local and local scales, the governing mechanisms at the atmosphere-surface continuum remain poorly understood. This area where the Sc cloud makes contact with the coastal topography represents a vast area in the desert, where processes such as dew formation and water vapor adsorption may significantly influence atmospheric humidity retention at the surface (Jacobs et al., 2006). These processes are key to understanding how life is sustained in such extreme environments. Moreover, the lack of integration between synoptic, local, and surface-scale dynamics limits our understanding of water and moisture pathways, their dynamics, and potential water budgets in hyperarid regions.

https://doi.org/10.5194/egusphere-2026-2396
Preprint. Discussion started: 20 May 2026

Given the multi-spatial scale complexity of atmospheric and surface mechanisms involved in transporting marine humid air into the desert, this research aims to unravel the main physical processes driving the transition from Sc to inland fog at the coastal Atacama. To address this, we conducted a field experiment called *StraToFog*, designed through a topographic transect to track the evolution of the MBL during an event of marine Sc cloud inland advection. In this manuscript, we describe the field experiment and present the first results of the main processes at non-local (MBL and Sc advection) and local (near-surface and surface) scales during the Sc-fog transition.

2 The *StraToFog* field experiment

2.1 Study site and measurement strategy

The *StraToFog* experiment was performed in the hyperarid coastal Atacama Desert, in the surroundings of the Alto Patache fog oasis (20.8° S, 71.1° W, ∼800 m ASL), between July 22^{nd} and August 3^{rd}, 2024. This period was chosen for its ideal conditions for fog advection (García et al., 2021). The Alto Patache site corresponds to a relic fog oases (Muñoz-Schick et al., 2001) mainly composed of a biological soil crust(Lehnert et al., 2018), which survives due to the persistent fog, present during 40% of the year (Keim-Vera et al., 2024). The oasis is located at the top of the coastal mountain range, a continuous steep mountain range that elevates parallel from the shore line up to 1500 m ASL over the first 15 km inland. In the surroundings of the oasis, landscape is characterized by bare land, with no plants on the surface, due to very low precipitation rates of < 5mm/year (Houston, 2006). Figure 1a shows an overview of the study area where the experiment was deployed.

The *StraToFog* field experiment was designed to measure the state of the MBL during the transition from Sc clouds to inland integrating non-local and local scales. To do so, we designed a transect from a ∼2 km offshore (A, Fig. 1) to 15 km inland (F, Fig. 1), where airborne measurements were performed simultaneously, and complemented with local meteorological observations and surface fluxes. Throughout the manuscript, we refer to non-local-scale measurements and processes constrained to the vertical variability of the MBL along the transect (15 km). In contrast, we refer to local-scale measurements and processes to the ones occurred within individual transect stations, including near-surface and surface measurements.

Figure 1a provides an overview map of the measurement sites deployed along the transect, and Figure 1b illustrates the measurement sites over the transect, from the ocean to the shoreline to inland. Every measurement site was divided into airborne, local and surface observations, of which instrumentation details are shown in Table 1. Airborne observations were conducted using radiosondes and UAVs, which were performed along the topographic transect at 2 km offshore (A) and 2 km (C), 3 km (D), 5 km (E), and 15 km (F) inland, respectively. In sites A, C, and F, radiosondes were released every two hours from 09:00 LT to 18:00 LT for two consecutive days (July 25-26^{th}, 2024) to measure air temperature, relative humidity, pressure, and wind components from ground level to at least 4,000 m above ground level (AGL; details in Table 1). In sites D and E, UAVs took off from the surface up to 500 m AGL every hour from 09:00 LT to 19:00 LT on the same days as radiosondes to measure vertical profiles of air temperature, air pressure, and relative humidity. Due to the limited flight altitude of the UAVs (up to 500 m AGL), we released these at 700 m ASL elevation to overcome the cloud layer (∼1,200 m ASL). Local routine

https://doi.org/10.5194/egusphere-2026-2396
Preprint. Discussion started: 20 May 2026

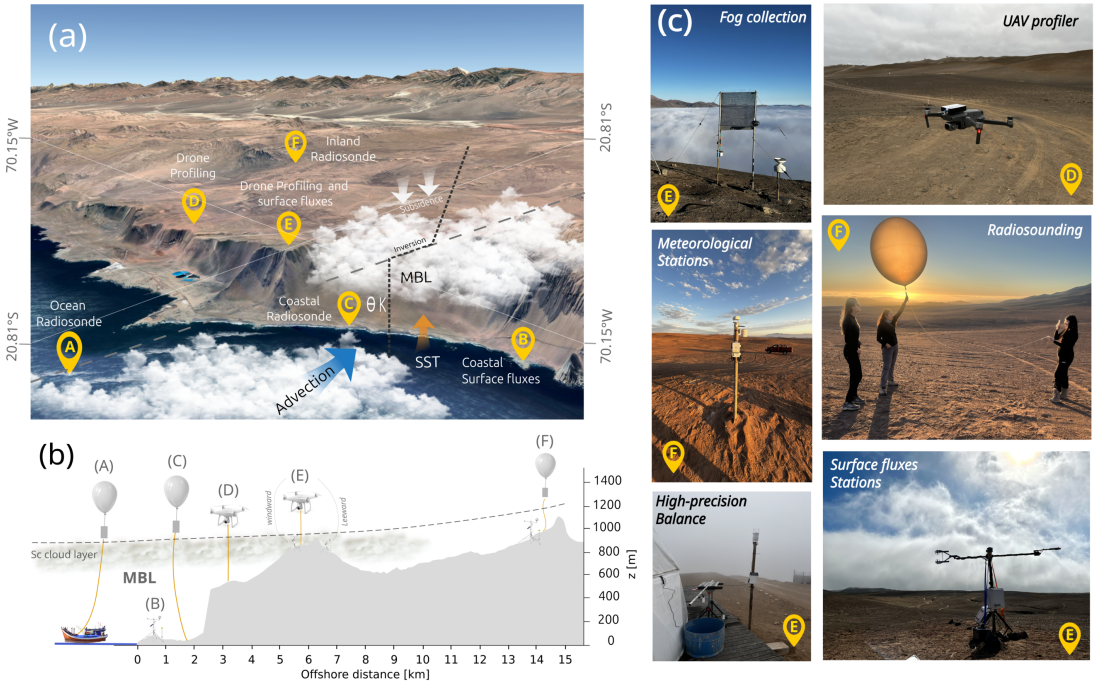

Figure 1. (a) Overview map in perspective of the deployment of measurement sites over the study area. (b) Schematic vertical cross-section of the measurement sites displayed over a transect from the near ocean to inland. (c) Photographs of instrumentation types used during the experiment.

meteorological observations were recorded at 10-minute intervals at sites B, E, and F between July 22^{nd} and August 3^{rd}, 2024. Monitored variables included 2 m air temperature, relative humidity, air pressure, and wind components (details in Table 1). In addition, fog water collection measurements were performed at site E using a standard fog collector (SFC, Schemenauer and Cereceda (1994)) at an identical temporal resolution. Three eddy covariance (EC) flux stations were installed at measurement sites B and E to monitor sensible and latent heat fluxes. The EC flux station at site B, was deployed at 5 m AGL, setting a measurement footprint over the beach. At site E, one EC station was deployed at the windward side of the mountain (at 2 m AGL), under the influence of fog, and a second one at the leeward side (2 m AGL), under the fog shade, which included net radiation and ground heat fluxes. Surface fluxes were computed by integrating 20-Hz raw data over 10-min intervals from July 23^{rd} to August 3^{rd}, 2024. Finally, over the same period, a high-precision balance was installed at site (E) to weigh a 35 x 45 cm soil sample, sheltered from the wind, and to measure atmospheric water deposition at 10-s resolution, with data aggregated into 10-min intervals. This setup included an infrared thermometer to measure the surface temperature of the soil sample and a meteorological station to measure air temperature, relative humidity, wind speed, solar radiation, and air pressure. Figure 1c shows photographs of every instrumentation type and location during the field experiment.

https://doi.org/10.5194/egusphere-2026-2396
Preprint. Discussion started: 20 May 2026

Spatial scale	Instrumentation type	Measurement point location	Date range	Time interval
Vertial	Radiosonde IMet4, Intermet Systems	(A): 20.85°S-70.24°W, 0 mASL (C): 20.85°S-70.15°W, 55 mASL (F): 20.72°S-69.96°W, 1004 mASL	July 25^{th}, 2024 July 25^{th}-26^{th}, 2024	2h (09:00 to 18:00 LT)
	UAV + IMetXQ2, Intermet Systems	(D): 20.74°S-70.14°W, 450 mASL (E): 20.81°S-70.15°W, 811 mASL		1h (09:00 to 19:00 LT)
Local	Meteorological station: ATMOS41 Meter Group.	(B): 20.89°S-70.13°W, 3 mASL (E): 20.82°S-70.14°W, 866 mASL (E): 20.81°S-70.15°W, 811 mASL (F): 20.72°S-69.96°W, 1004 mASL	July 22^{nd}- August 3^{rd} 2024	10 minutes
	Standard Fog Collector (SFC)	(E): 20.82°S-70.14°W, 866 mASL		
Surface	Eddy covariance system: - LI-710, Licor - IRGASON, Campbell Sci. - A 1g precision weight (Midrics 1 MW1, Sartorius, Germany) Infrared temperatur sensor (IRT), Apogee	(B): 20.89°S-70.13°W, 3 mASL (C): 20.85°S-70.15°W, 55 mASL (E): 20.82°S-70.14°W, 866 mASL (windward) (E): 20.80°S-70.13°W, 665 mASL (leeward)	July 22^{nd}- August 3^{rd}	20 Hz averaging in 10 min 10 seconds integrated in 10 min

Table 1. Detail of the instrumentation, localization and time interval ranges used during the *StraToFog* field experiment along the transect shown in Figure 1b.

2.2 Synoptic conditions during *StraToFog*

The coastal Atacama Desert is well-known for being under the influence of the South-eastern pacific anticyclone, a quasi-permanent and vigorous high-pressure system derived from the downward branch of the Hadley cell, which impedes vertical cloud formation. Despite this, the high pressure exhibits regular anomalies, which affect the Sc cloud height level. Figure 2 shows the synoptic conditions observed during the *StraToFog* field experiment, which were characterized by a high-pressure condition from July 22^{nd} to 24^{th} (1019 hPa at sea level), transitioning during two days into a lower-pressure condition (1013 hPa at sea level) from July 27^{th} to August 3^{rd}. Airborne measurements were taken over this transition period between the two opposing pressure conditions, while local and surface measurements were taken during both conditions. Figure 2c and 2d reinforce the contrasting pressure conditions, showing a positive mean surface pressure level (MSPL) anomaly between 2 and 2.5 hPa on July 24^{th}, and a negative anomaly between -0.5 and -1 hPa on July 30^{th} over the entire coastal area of the Atacama. Figures 2e and 2f illustrate the effect that the pressure anomaly has on the Sc cloud in the study area. As shown in the photograph in Figure 2e, taken on July 24^{th}, the Sc cloud top was located below the site E, from where the photograph was taken, at 866 m ASL (Fig. 1). A few days later (Fig. 2f), at the same site, the cloud base level was located above site E, which demonstrates that pressure systems can vary the Sc cloud layer level by dozens of meters in a few days. This variation in the Sc cloud layer has an impact on fog water collection rates, as shown in Figure 2b. Figure 2b illustrates discontinuous water collection during high-pressure conditions, as the cloud was mostly below the fog collector. In contrast, during lower-pressure conditions, fog collection became more regular.

https://doi.org/10.5194/egusphere-2026-2396
Preprint. Discussion started: 20 May 2026

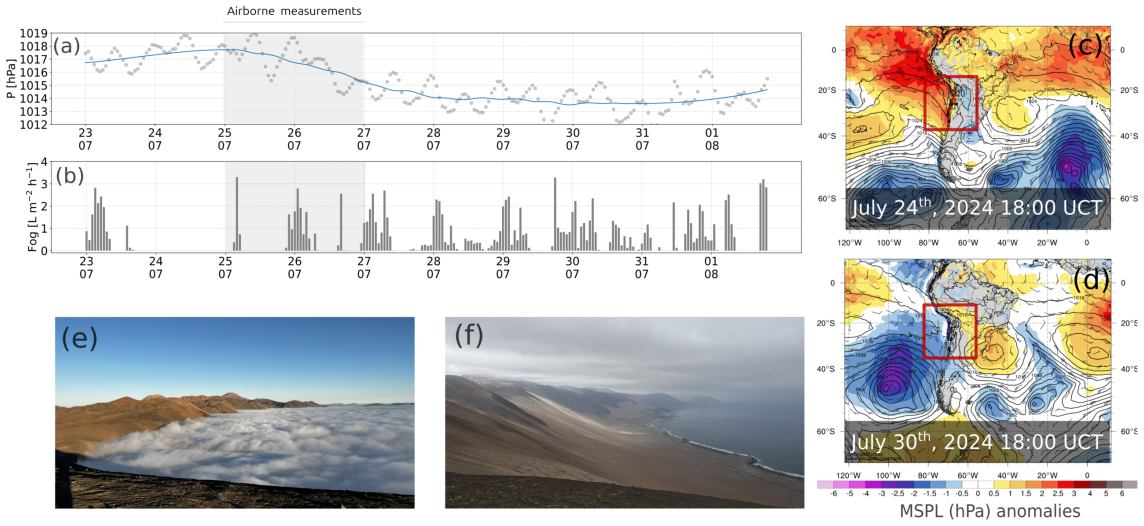

Figure 2. Synoptic conditions during the *StraToFog* experiment. (a) Air pressure time series measured at 5 m ASL in site (B). The solid blue line represents the moving average. (b) Fog water collection measured by a standard fog collector at the site (E) windward location. The saded time period correpsond to the days where airborne measurements were performed. (c, d) Mean surface pressure level anomalies over the study area (red square) for July 24^{th} and 30^{th}, taken from: https://www.atmos.albany.edu/student/abentley/index.html. (e, f) photographs of Sc cloud layer taken at the site (e) on July 24^{th} and 30^{th}.

3 Results

The dataset from the StraToFog field experiment allows studying the Sc cloud-to-land fog transition across multiple spatial scales. In this section, we focus on the non-local scale as a first-order perspective. Specifically on vertical measurements that describe the diurnal variability of the MBL during the marine Sc-fog inland advection (3.1). Afterwards, as a second-order perspective, we shift the focus to the local scale by first characterizing the thermodynamic state of the atmosphere on the main transect points during several fog events (3.2). Finally, to delve into local-scale processes, we focus on the surface by describing the impacts of fog deposition, dewfall, and water vapour adsorption, as surface fluxes that enable atmosphere-surface mass exchange (3.3).

3.1 Non-local scale perspective: the MBL diurnal evolution and inland advection

Figure 3 shows the diurnal evolution of the vertical profiles of potential temperature (θ), mixing ratio (q), wind speed (U) and adiabatic liquid water content (ql) measured by radiosondes launched at site B on July 26^{th}, 2024. In general terms, the MBL shows an averaged diurnal height of 810 m, with a typical well-mixed profile (Fig. 3a) around 289 K, and a thermal inversion

https://doi.org/10.5194/egusphere-2026-2396
Preprint. Discussion started: 20 May 2026

layer around 15 K. The MBL height evolves throughout the day from 770 m at 08:00 LT, increasing rapidly at a rate of 2.5 cm s^{-1} until reaching 950 m at 12:00 LT. In the afternoon, the MBL height drops at 1.6 cm s^{-1} to 800 m at 14:00 LT, then increases again to 920 m at 16:00 LT. Finally, the MBL drops rapidly at 3 cm s^{-1} until it reaches 710 m at 18:00 LT. The MBL mixed-layer (θ) shows a slow and subtle diurnal increase in temperature from 286 K to 290 K. However, this warming is not entirely homogeneous throughout the well-mixed layer. It starts at the top of the MBL, as shown in Figure 3a, between 600 and 800 m at 10:00 LT and 18:00 LT. This upper-level warming is associated with MBL growth, for example at 12:00 LT, when the layer reaches its maximum height (950 m) and θ increases throughout the MBL, indicating that warming is driven by entrainment at the MBL top. In contrast, the lower part of the mixed layer remains colder over the first 200 m, consistent with the shading effect of Sc clouds (Fig. 3d) on the surface, particularly from 08:00 LT to 10:00 LT and from 16:00 LT to 18:00 LT. The thermal inversion layer also varies throughout the day (white area in Fig. 3a). At 08:00 LT, it is sharp (19 K) between 800 and 900 m. From 10:00 to 14:00 LT, the inversion weakens to 15 K and extends between 700 and 1000 m ASL. At 16:00 LT, it strengthens again to 17 K before decreasing to 11 K at 18:00. The vertical profile of q shows a similar patterns (Figure 3b), with an average MBL humidity of 7.2 g kg^{-1}. Humidity first increases near the surface (0-200 m) and then throughout the entire well-mixed layer, rising from 6 to 8 g kg^{-1} at a rate of $\sim$0.2 g kg^{-1} h^{-1}. This increase in q is related to observed U (Fig. 3c), which rises after 12:00, and peaks at around 4 m s^{-1} at 16:00 LT (from the SW), indicating moisture advection from the ocean. The sea breeze observed in Figure 3c corresponds to a thermally driven wind caused by the contrast between the cool ocean and the hot desert, typical to the Atacama (Rutllant et al., 2003; Lobos-Roco et al., 2021). Figure 3d shows the adiabatic liquid water content (q_l), estimated as the positive difference between the mixing ratio (q) and the saturated mixing ratio (q_s) along the vertical profile (Wetzel, 1990; Duynkerke et al., 1996). This variable represents the over saturated MBL air and, thus, the Sc cloud water density. Overall, q_l increases almost linearly from 650 up to 920 m, reaching a maximum of approximately 0.5 g kg^{-1} at the cloud top at 16:00. This value is consistent with previous observations in Atacama Sc cloud in (Schween et al., 2022) and over the north Atlantic Ocean (Duynkerke et al., 1996). Figure 3d also shows the diurnal cycle of Sc cloud formation and dissipation. Clouds form in the morning at 08:00 LT and dissipate by 10:00 LT. From noon to 16:00 LT, Sc clouds form again, increasing in depth from 127 to 267 m while the lifting to the cloud top height of 877 m. By 18:00 LT, cloud tops descend to about 707 m, and cloud depth decreases to 107 m.

To further examine the vertical dynamics of the Sc cloud shown in Figure 3d, Figure 4 presents the dynamics of the cloud base (CB), estimated as lifting condensation level from surface observations and radiosondes, and the cloud top (CT), estimated from MBL heights measured by radiosondes and UAVs during July 25^{th} and 26^{th}, 2024. Figure 4a shows the CB at sites B, C and D as blue dots and the CT at sites C, D, E and F as black dots. Overall, from the shoreline to 2 km inland, we observe a different dynamic of the cloud layer between the night and early morning, and between the afternoon and the evening. Figure 4b represents these dynamics between the CB and the CT during the night and early morning. During the morning, the CB rises slightly (<50 m) between 0 and 2 km inland but then lowers by approximately 100 m between 2 and 3 km. In contrast, the CT between 2 and 3 km inland remains nearly constant, without any significant vertical variations.

CT remains stable due to the strong inversion layer shown in Figure 3a ($\sim$19 K), which inhibits vertical MBL growth. During

https://doi.org/10.5194/egusphere-2026-2396
Preprint. Discussion started: 20 May 2026

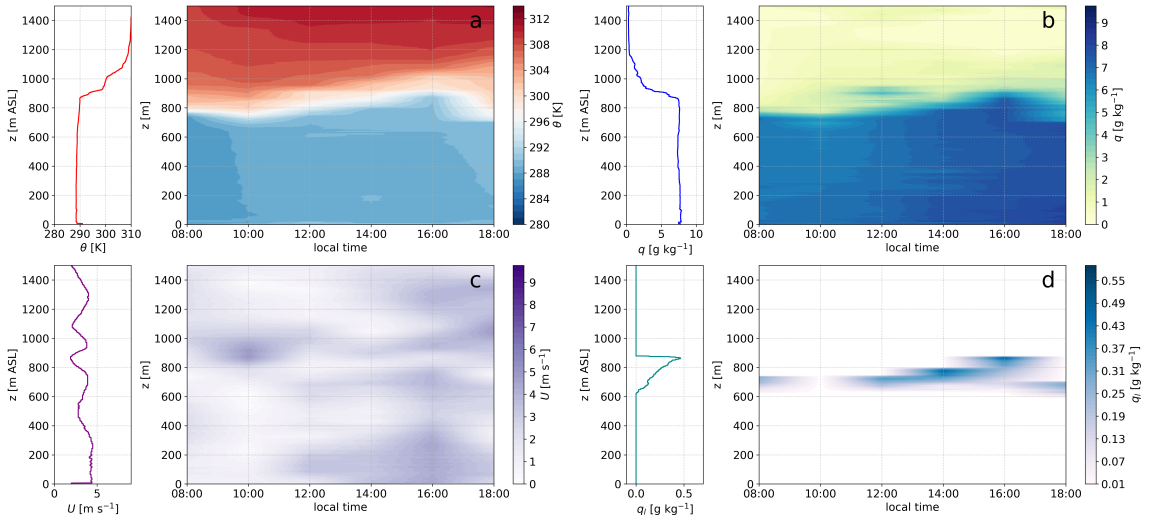

Figure 3. Diurnal evolution of vertical profiles of (a) potential temperature, (b) mixing ratio, (c) wind speed and (d) adiabatic liquid water content, measured at site (B) on July 26^{th}, 2024. The vertical profile attached to each subfigure corresponds to the one measured at 16:00 local time.

the afternoon and towards the evening, increasing sea to land wind speed modify the cloud layer dynamics, resulting in the lifting of both the CB and CT. Figure 4c schematizes this cloud layer vertical-and-inland dynamics between the afternoon and the evening. First, CB lifts by ∼100 m between 0 and 2-3 km inland as it encounters the topographic "wall". Similarly, CT increases abruptly by ∼400 m from 2-3 km to 5 km inland, reaching 1200 m ASL. Farther inland (15 km), the CT descends again to ∼1100 m ASL, following the mountain topography. This lifting of the CB is driven by the topography through two mechanisms. First, MBL warming (Fig. 3a) increases the boundary layer height above the mountain summits, allowing it to move farther inland. This dynamic is produced by the activation of the afternoon sea breeze (Fig. 3c), which promotes moisture advection (Fig. 3b), maintaining the Sc cloud during its inland transition. Second, surface heating by solar radiation further deepens the MBL and raises the lifting condensation level, contributing to the observed increase in CB height.

Finally, to delve into the thermodynamic changes in the MBL during the inland transition, Figure 5 shows the vertical profiles of θ and q measured on July 26^{th} 2024, at 16:00 LT at sites C, E, and F, located at 2 km, 5 km, and 15 km offshore, respectively. Figure 5a shows that, from near-shore (2 km) to inland, θ profiles have the same shape; however, since the sites located 5 and 15 km inland were situated at higher elevations along the topographic transect, their profiles start at higher altitudes. The profiles taken at 2 and 5 km are nearly identical when overlapped, showing the same mixed-layer potential temperatures and inversion layer heights. In contrast, the site located 15 km inland shows a shorter inversion layer at 1100 m ASL, characterized by a colder free troposphere than the near-shore sites. Despite these differences, the mixed-layer potential temperature remains close to near-shore values (∼290 K), indicating that the advected MBL replaces the inland air rather than mixing with it as it is moves inland from the ocean. Figure 5b shows a humidity structure similar to θ for the three different sites. However, we

https://doi.org/10.5194/egusphere-2026-2396
Preprint. Discussion started: 20 May 2026

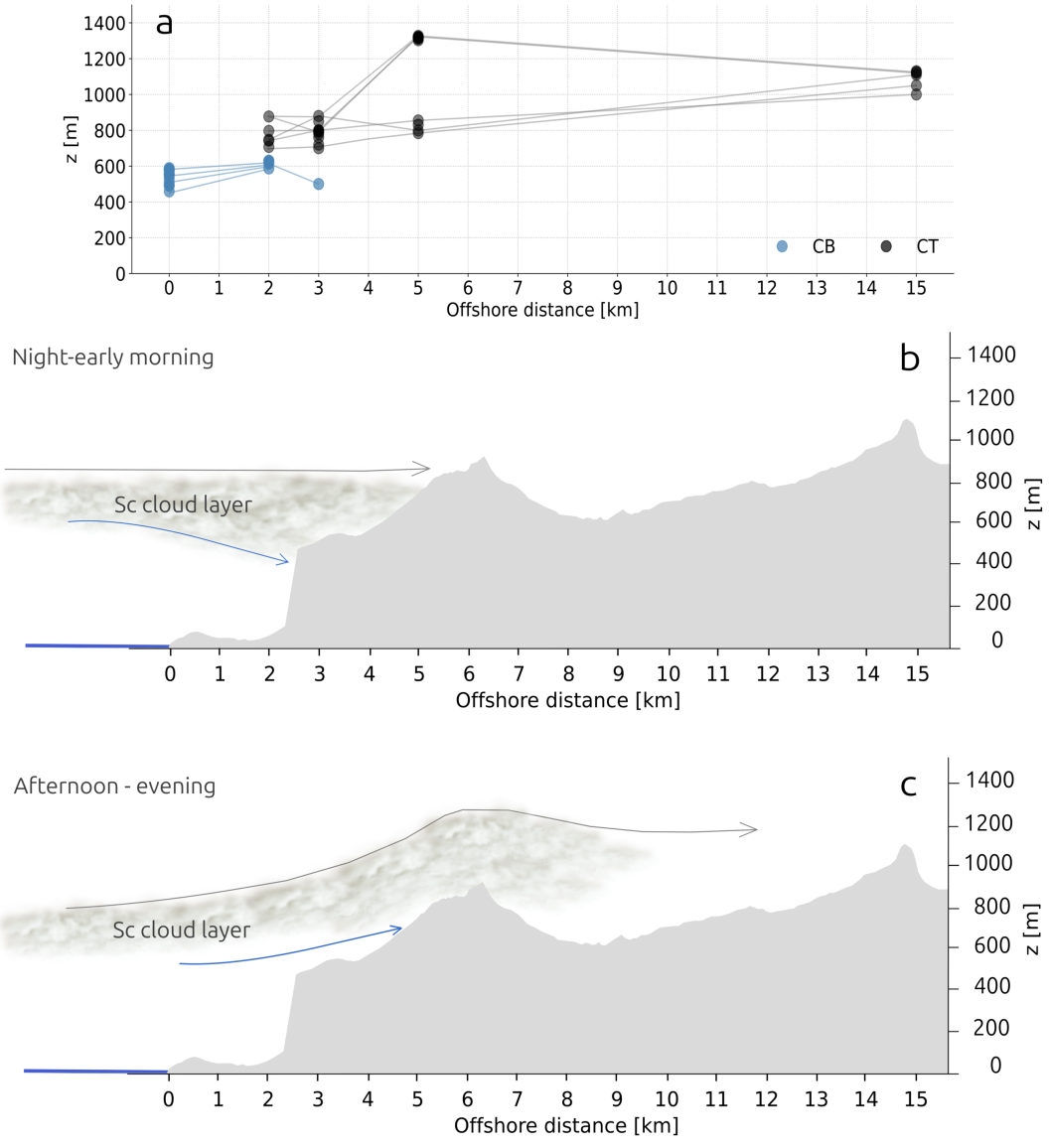

Figure 4. (a) Cloud base (CB, blue) and cloud top (CT, black) height measured by radiosondes and UAVs in sites A to F on July 26^{th}, 2024. (b) Schematic vertical cross-section representing the CB lowering during the night and early morning. (c) Schematic vertical cross-section representing the CT topographic up lifting during the afternoon and evening.

https://doi.org/10.5194/egusphere-2026-2396
Preprint. Discussion started: 20 May 2026

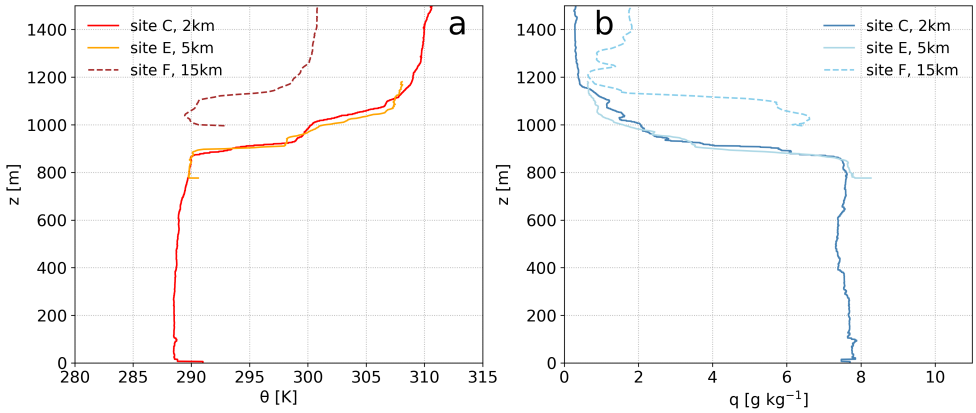

Figure 5. Vertical profiles of (a) potential temperature (θ) and (b) mixing ratio (q) measured simultaneously by radiosondes and UAVs on July 26^{th}, 2024 at 16:00 LT over sites C (2 km offshore), E (5 km offshore) and F (15 km offshore).

observe two remarkable patterns. The first is that the mixed-layer q differs between the sites located 2 and 5 km ($\sim$7.5 g kg^{-1}) and 15 km inland (6.0 g kg^{-1}). This reduction in q when θ remains isothermal within the MBL during the inland advection suggests that atmospheric humidity is being retained in the coastal mountains (2 to 5 km inland). Since the maximum adiabatic liquid water content (q_l) observed at 16:00 LT (Fig. 3d) is $\sim$0.5 g kg^{-1}, and the reduction in q is 1.5 g kg^{-1} over the mixed-layer, the mountains are most likely retaining not only liquid water (fog), but also at least 1 g kg^{-1} of water vapor along the MBL vertical profile. The second unexpected pattern is the difference in q at the surface layer (the first meters above ground) between the sites located 2 and 5 km inland. The ground at the site located 2 km inland is drier than the well-mixed layer, whereas the ground at the site located 5 km inland is wetter than the well-mixed layer aloft. This wet air near the surface in a hyperarid region could indicate that fog deposition and evaporation are occurring, moistening the air very close to the surface at site E (5 km inland).

3.2 Local scale perspectives

3.2.1 The thermodynamic state of the atmosphere under advective fog events

To complement the analysis of MBL advection, we describe and analyse the thermodynamic state of the atmosphere at the local scale near the surface (2 m above the ground), during typical fog events.

Figure 6 shows the temperature (T), relative humidity (RH), and wind speed (U) measured in meteorological stations located along the transect at sites B, E, and F, respectively, during the *StraToFog* field experiment. At site B, located 2 km offshore (Fig. 6a), RH is around 80% with little diurnal variation, while temperature varies slightly between 14 and 17 °C. The U is generally low, ranging from 1 to 5 m s^{-1}. This station shows typical low diurnal variability due to its proximity to the ocean and low elevation. At 866 m ASL in site B (5 km offshore, Fig. 6b), we observe a more marked diurnal variability, with RH values

https://doi.org/10.5194/egusphere-2026-2396
Preprint. Discussion started: 20 May 2026

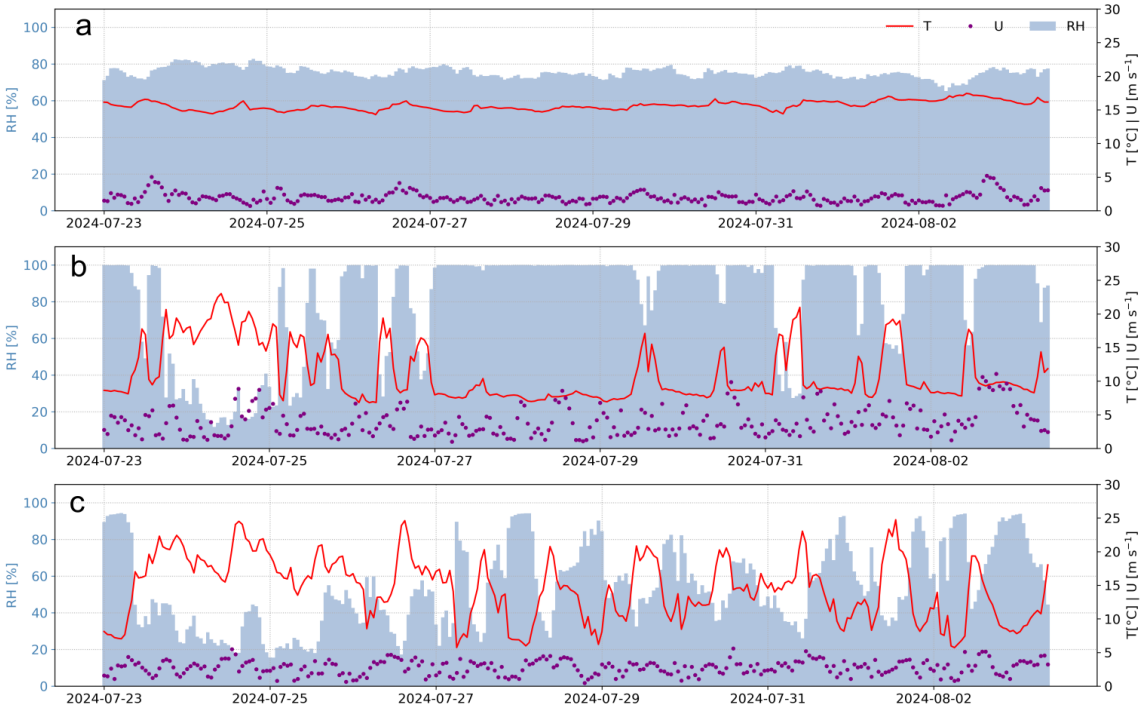

Figure 6. Time series of air temperature (T), relative humidity (RH) and wind speed (U),measured at 2 m from the ground in sites (a) B (2 km offshore), (b) E (5 km offshore) and (c) F (15 km offshore) between July 23^{rd} and August 2^{nd}, 2024.

reaching 100% every day between July 25^{th} and August 3^{rd}. Temperature also shows a more marked diurnal variability and U is higher compared to site B, ranging from 1 to 11 m s^{-1}. This change is probably due to the position of site E on the transect, which is located at the same height as where the Sc cloud intersects the topography, therefore forming fog. Finally, site F (Fig. 6c), located at 1100 m ASL and 15 km offshore, shows well-marked diurnal variability in both RH and temperature, with low temperatures coinciding with high RH, as a result of the advected MBL analysed in section 3.1. At site F, U decreases again to maximum values < 5 m s^{-1}. In Figures 6b and 6c, a noticeable dry condition is observed from July 23^{rd} to 25^{th}, which is absent in Figure 6a. This difference is due to the high-pressure conditions observed during the first days of the field experiment, when the MBL dropped below 600 m ASL, leading to predominantly desert conditions at sites E and F, as shown in Figure 3. Finally, the differences found in U between sites, in which there are higher speeds in site E than in site F are most likely due to the location of site E, which coincides with where the interaction between the cool MBL, the hot air over the desert, and the inversion capping produces topographic-atmospheric channelling (Lobos-Roco et al., 2021).

To examine thermodynamic changes at the local scale during fog events, we focus on site E, where Figure 7 illustrates a typical diurnal cycle observed during the *StraToFog* field experiment. Two main fog regimes are identified (Figures 7a and 7b): a night-early morning regime (00:00 - 09:00) and an afternoon-evening regime (15:00 - 23:00). During the morning, relative

https://doi.org/10.5194/egusphere-2026-2396
Preprint. Discussion started: 20 May 2026

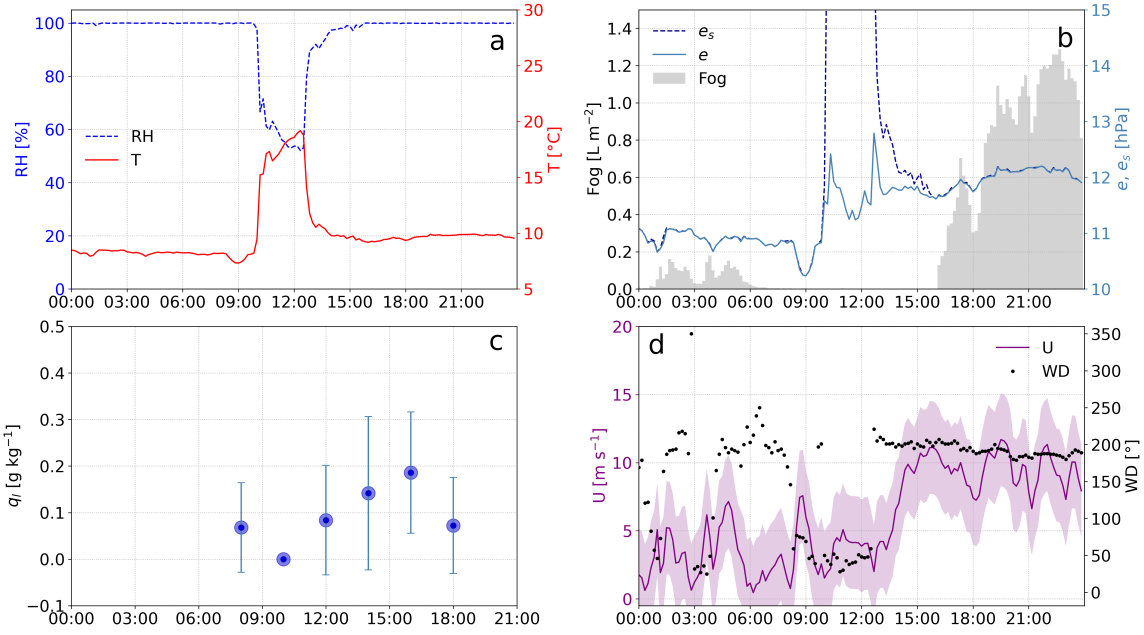

Figure 7. Diurnal cycle of (a) air temperature and relative humidity, (b) fog collection, vapor pressure and saturated vapor pressure, (c) adiabatic liquid water content, and (d) wind speed and wind direction measured on July 26^{th}, 2024 at 16:00 LT over site C approximately at 860 m ASL (5 km offshore). The adiabatic liquid water content correspond to the one obtained by the radiosonde launched at site C (Fig. 3c), which is not always in agreement with observations taken at site E shown in subfigures a, b and d.

humidity (RH) reaches 100% with air temperatures around 6 °C (Fig. 7a), indicating (over) saturated conditions conductive to fog formation at the site E. Figure 7b shows fog collection, vapor pressure (e), and saturated vapor pressure (e_s), with water volumes of around 0.1 L m^{-2} every 10 minutes and both e and es near 10.7 hPa. The morning and afternoon regimes are separated by a non-fog period between 09:00 and 14:00 LT, during which temperature increases sharply from 6 to 20 °C and RH decreases to about 50%. The afternoon regime is characterized by RH close to 100%, similar to the morning regime, and higher temperatures, with a mean of 10 °C. During this period, the intersection between e_s and e occurs at higher values than in the morning, reaching 12.3 hPa. The most remarkable difference between the morning and afternoon regimes is fog collection, which increases by one order of magnitude during the afternoon, reaching a rate of 1.2 L m^{-2} every 10 minutes. To further investigate this difference, Figure 7c presents the adiabatic liquid water content (q_l), which is higher in the afternoon (0.2 g kg^{-1}) than in the morning (0.08 g kg^{-1}). Figure 7d shows the diurnal wind regime, with calm winds of 2.5 m s^{-1} from the South-Southwest (SSW) during the morning fog period. These winds shift rapidly to East winds during the non-fog time period at midday. During the afternoon regime, wind speed (U) increases up to 10 m s^{-1} from the SSW.

https://doi.org/10.5194/egusphere-2026-2396
Preprint. Discussion started: 20 May 2026

3.2.2 Water-energy exchange between humid marine air and the dry surface

The thermodynamic state of the near-surface atmosphere during an advective fog event interacts with the surface, leading to mass and energy exchange. Figure 8 presents the diurnal cycle of accumulated atmospheric water (AW) deposition measured by a high-precision balance (Fig. 1c, site E) compared to atmospheric relative humidity (RH), surface temperature (T_s), and atmospheric dew temperature (T_{dew}), and fog collection, averaged over several fog events between July 25^{th} and August 2^{nd}, 2024. As shown in Figure 8a, atmospheric water deposition exhibits diurnal variability as a response to different physical processes at the surface. For example, over the night (03:00 to 06:00), AW reaches its maximum value (0.18 mm) when air is not saturated (RH<100%) and $T_s \sim T_{dew}$ (Fig. 8b). This AW deposition is interpreted as dewfall, since the values of RH and T_s-T_{dew} indicate that the near-surface air is not condensing (i.e., fog), even though the fog collector (located at 2 to 3 m AGL, and 1 km from the balance) shows low but nonzero collection values (Fig. 8c). During the morning (06:00 to 12:00), the accumulated AW deposition decreases sharply, indicating that the weight measured by the high precision balance is decreasing, which means surface evaporation. This decrease is in agreement with RH < 100%, a large difference between T_s and T_{dew}, and the lower fog collection rates. At the afternoon, from 12:00 to 20:00 LT, the accumulated AW deposition increases gradually, while RH remains between 70% and 85%, and T_s-T_{dew} remains large. We interpret this increase in AW as water vapor absorption by the desiccated surface following morning evaporation. Between 19:00 and 20:00 LT, AW deposition in Figure 8a shows a slight decrease just before RH reaches 100%. We interpret this brief evaporation as a phase change from atmospheric saturated water vapor to liquid water in the air (fog), which releases latent heat as sensible heat, warming the surface (Fig. 8b). After that, the air oversaturates (RH > 100%), and AW increases sharply, indicating fog deposition onto the surface. The AW inputs throughout the diurnal cycle described above are difficult to distinguish with a single instrument. However, by correlating AW deposition with atmospheric variables such as RH, T_s and fog collection, we can distinguish several processes. For example, Figure 8d shows the relationship between AW deposition and RH coloured by T_s. Within this positive correlation, water vapor adsorption can be distinguished at RH values of ~85%, whereas fog and dew occur at RH > 90%, both under low T_s conditions. Likewise, Figure 8e shows the correlation between AW deposition and T_s coloured by RH. A strong inverse-exponential relationship is evident, suggesting that AW deposition may be reliably predicted by T_s. When considering RH values, fog (RH = 100%) and dew (RH ~90%) can be distinguished at low T_s and high AW levels. Finally, Figure 8f shows a positive, although scattered, correlation between AW deposition and fog water collection, coloured by RH. This relationship further distinguishes fog (RH = 100%) from dew (RH < 100%) within the regime of high AW deposition and fog collection.

To further characterize mass and energy exchange between the atmosphere and the dry surface during the experiment, Figure 9 presents the averaged diurnal cycles of sensible (H) and latent (LE) heat fluxes measured at sites B (shoreline), and E-windward and E-leeward, located 5 and 6 km offshore, respectively (Fig. 1b). The surface fluxes observed within the MBL at site B (Fig. 9a) are relatively weak, with both H and LE maximum values around 50 W m^{-2}. Both fluxes start to increase at midday, coinciding with the afternoon wind regime (Fig. 7d). This suggests that surface fluxes at the coast are triggered by mechanical turbulence once sea-land breeze is activated. The weak observed fluxes are driven by low radiation

https://doi.org/10.5194/egusphere-2026-2396
Preprint. Discussion started: 20 May 2026

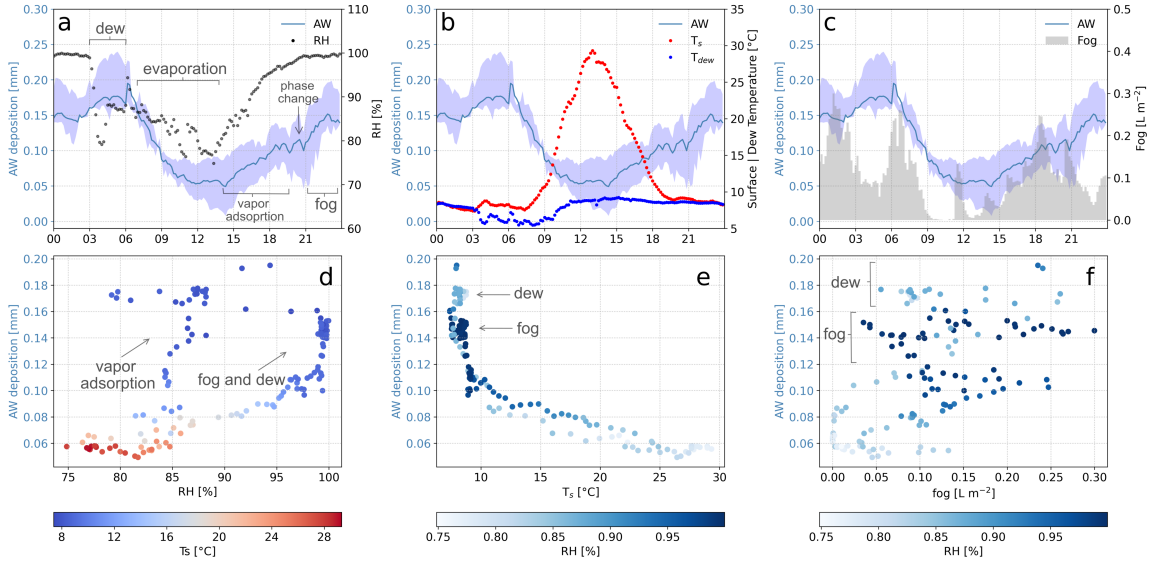

Figure 8. Top panels: averaged diurnal cycle of accumulated atmospheric water (AW) deposition on surface measured by the high-precision balance compared to (a) air relative humidity (RH), (b) surface (T_s) and air dew temperature (T_{dew}), and (c) fog water collection between July 25^{th} and August 2^{nd}, 2024 at site E. Bottom panels: correlation between (d) AW deposition and RH, (e) AW deposition and T_s, and (f) AW deposition and fog collection.

underneath the Sc cloud cover and by a MBL cooling caused by cloud-topped radiative lost. Site E is divided into two points: E-windward (Fig. 9b), at 866 m ASL, facing the ocean, where Sc cloud is intercepted by topography, and E-leeward (Fig. 9c), at 665 m ASL, facing the desert to the East of the mountain (See Fig. 1b). For both E-site flux stations, H follows the diurnal cycle of temperature (Fig. 6b,c), with a clear fog effect at the E-windward site, which shows more variability (std: 23 W m^{-2}, max: 230 W m^{-2}) compared to the E-leeward site (std: 13 W m^{-2}; max: 300 W m^{-2}). In contrast to site B at the coast, the diurnal variability of H at both E sites suggests a thermal (buoyant) origin of turbulence. Regarding LE at both E sites (Figs. 9b, c), there are similar diurnal variabilities in accumulated AW deposition (Fig. 8), suggesting a positive relationship between upward and downward LE fluxes and surface AW deposition. For example, the LE shown in Figure 9c is ∼-5 W m^{-2} between 03:00 and 06:00 LT, which is in agreement with the dewfall observed in Figure 8a. From 06:00 to 12:00 LT, LE increases to 20 W m^{-2}, reinforcing the morning surfacewater evaporation observed in the high-precision balance. From 12:00 onward, LE decreases to negative values, reaching -15 W m^{-2} around 18:00 LT. The negative values of LE with positive and relatively high values of H, reinforce the idea of water vapor adsorption during the afternoon. Finally, from 20:00 LT onward, LE increases again toward near zero values due to fog.

https://doi.org/10.5194/egusphere-2026-2396
Preprint. Discussion started: 20 May 2026

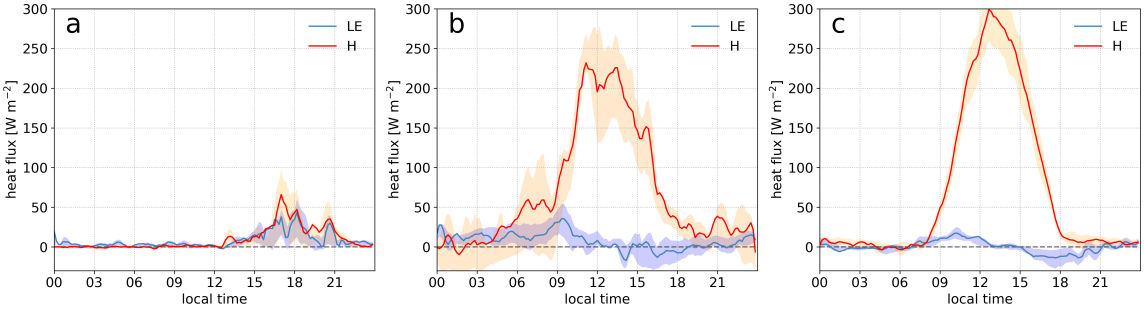

Figure 9. Averaged diurnal cycle of sensible (H) and latent (LE) heat fluxes on sites: (a) B, (b) E-windward, 5 km offshore, and (c) E-leeward, 6 km offshore between July 25^{th} to August 2^{nd}, 2024.

4 Synthesis of the main findings

The analysis of non-local (vertical), and local (near surface and surface) observations collected during the *StraToFog* field experiment allows us to develop a physically based explanation of the processes triggered when the humid marine cloud-topped boundary layer is advected over the hyperarid surface of the Atacama. Figure 10 presents a schematic vertical cross-section from the nearshore to 15 km inland, illustrating the interaction between the humid marine atmosphere and the dry land during the marine stratocumulus-to-fog transition.

Figure 10a shows the Sc-fog transition zone during the night. Here, a well-mixed MBL forms under a strong thermal inversion ($\Delta\theta$ = 19 K), sustaining a thin yet persistent Sc cloud deck in contact with the coastal topography, and producing fog over land at 770 m ASL. The sea-land breeze weakens as it is counteracted by the weak land-sea breeze produced by katabatic downslope winds (Muñoz et al., 2013).

At night, fog forms on the windward mountain slope, where oversaturated air is induced by atmospheric cooling; then e_s decreases to reach e (Fig. 7b). This condensation forms fog with low liquid water content, which combined with weak winds, yield low fog collection rates. At the leeward mountain slope, the MBL remains trapped, although unsaturated (RH<100%), producing downward LE that forms dew at the surface. From morning to noon (Fig. 10b), the MBL heats up, decreasing $\Delta\theta$ and thereby allowing dry air entrainment at its top (RH ~50%), which produces temporal Sc breaks. These temporal breaks are alternated by Sc cloud lowering near the mountain slope due to humid air accumulation at the slope. In the morning, the land-sea breeze dominates (Fig. 7d), bringing dry air from the inland desert that dissipates fog (e_s-e >> 0, Fig. 7b). As a consequence of fog dissipation, air temperature, as well as H and LE increase, producing surface evaporation of nighttime dewfall accumulation (Fig. 8a). Finally, from the afternoon to evening (Fig. 10c), the sea-land breeze is activated, promoting the MBL inland advection. This sea-land breeze triggers several processes in the Sc-fog transition zone. First, at the sea level, surface fluxes of H and LE are activated due to wind shear (Fig. 9a), which produces mechanical turbulence. Second, the Sc cloud layer is forced to uplift ~400 m due to the topographic barrier (Fig. 4a), increasing wind speed at the local scale through wind channelling. This uplift of the Sc cloud, accompanied by ocean moisture advection (Fig. 3b), increases the liquid water

https://doi.org/10.5194/egusphere-2026-2396
Preprint. Discussion started: 20 May 2026

content (Fig. 3c), as e increases until it reaches e_s at higher pressure (and temperature; Figs. 7a and 7b). Increases in wind speed and liquid water content trigger elevated fog water collection rates (Fig. 7b) (Montecinos et al., 2018). Finally, at the leeward mountain slope, MBL advection transports moisture to the recently desiccated surface, which starts to adsorb water vapor while the air remains undersaturated (RH ~75%) and T_s-T_{dew} >> 0, resulting in negative LE fluxes (Fig. 9c). Later in the evening, advective fog dominates the windward and the leeward slopes, producing surface fog deposition (Fig. 8). This deposition occurs under saturated air and surface (RH: 100%, T_s-T_{dew} = 0 °C) and, due to wind speed, near-zero LE. The negative LE, resulting from the afternoon AW deposition (vapor adsorption and fog), reduces the MBL humidity budget in approximately 1.5 g kg^{-1}, when it reaches 15 km inland (Fig. 5).

Several of the processes mentioned above have been studied and observed in the Atacama and other arid regions on Earth. The marine Sc vertical structure was well-studied through observations by Duynkerke et al. (1996) in the North Atlantic, showing a cloud depth of ~200 m and a maximum q_l of 0.6 g kg^{-1} along the vertical profile. Both these results agree with our findings, where Sc cloud depth ranged from 127 to 265 m, and the maximum q_l was 0.5 g kg^{-1}. In the coastal Atacama region, Schween et al. (2022), using a temperature profiler combined with a cloud radar, measured the same maximum q_l as we did during our field experiment. Regarding Sc cloud advection, Malik et al. (2026) observed a similar lowering of Sc cloud base over the coastal topography of the Namib Desert by around 200 m, compared with the ~100 m observed in our experiment. In the Atacama, the inland Sc cloud uplifting observed in our radiosoundings has been previously reported by del Del Río et al. (2021) during the GOFOS experiment, where CT measured at 12 km inland were located between 1000 and 1400 m ASL, approximately 400 m higher than those observed at the coast. The vigorous sea-land breeze observed in the afternoon, which results from the thermal differences between the cool ocean and the hot desert, has also been previously reported by Lobos-Roco et al. (2021). Finally, the night-morning eastern winds observed during the experiment have been reported by Rutllant et al. (2003) as a returning cell of the sea-land breeze, which collapses during the night and returns to the coast (land-to-sea) during the morning.

Besides the well-documented vertical structure of Sc cloud in the Atacama and other similar coastal regions, the thermodynamic state of the atmosphere during advective fog events has rarely been documented in detail. Lobos-Roco et al. (2018) and García et al. (2021) describe the stability within the MBL using meteorological stations during fog formation-dissipation events in the coastal Atacama. Likewise, fog collection has been widely studied in the Atacama by Cereceda et al. (2000, 2002, 2008), Larrain et al. (2002), del Río et al. (2018), and Lobos-Roco et al. (2025), all of whom reported similar fog collection values and diurnal variability to the ones observed during the *StraToFog* experiment. Finally, Keim-Vera et al. (2024) reported a high-fog collection efficiency during orographic fog in the coastal Atacama, associated with high wind speed in the afternoon, which is in agreement with the afternoon fog regime observed during the experiment.

Despite the characterization of the vertical structure of the MBL and the local atmospheric state during fog collection, these scales have never been linked to each other or to processes at the surface, such as dewfall, fog deposition, and water vapor adsorption. However, several authors report such processes in different arid regions of the Earth. For example, Jacobs et al. (1999, 2006) and Heusinkveld et al. (2006), using low-cost micro-lysimeters in the Negev Desert, reported accumulated dew deposition of 0.25 mm, similar to the 0.18 mm of AW deposition observed during the *StraToFog* experiment. Finally, negative

https://doi.org/10.5194/egusphere-2026-2396
Preprint. Discussion started: 20 May 2026

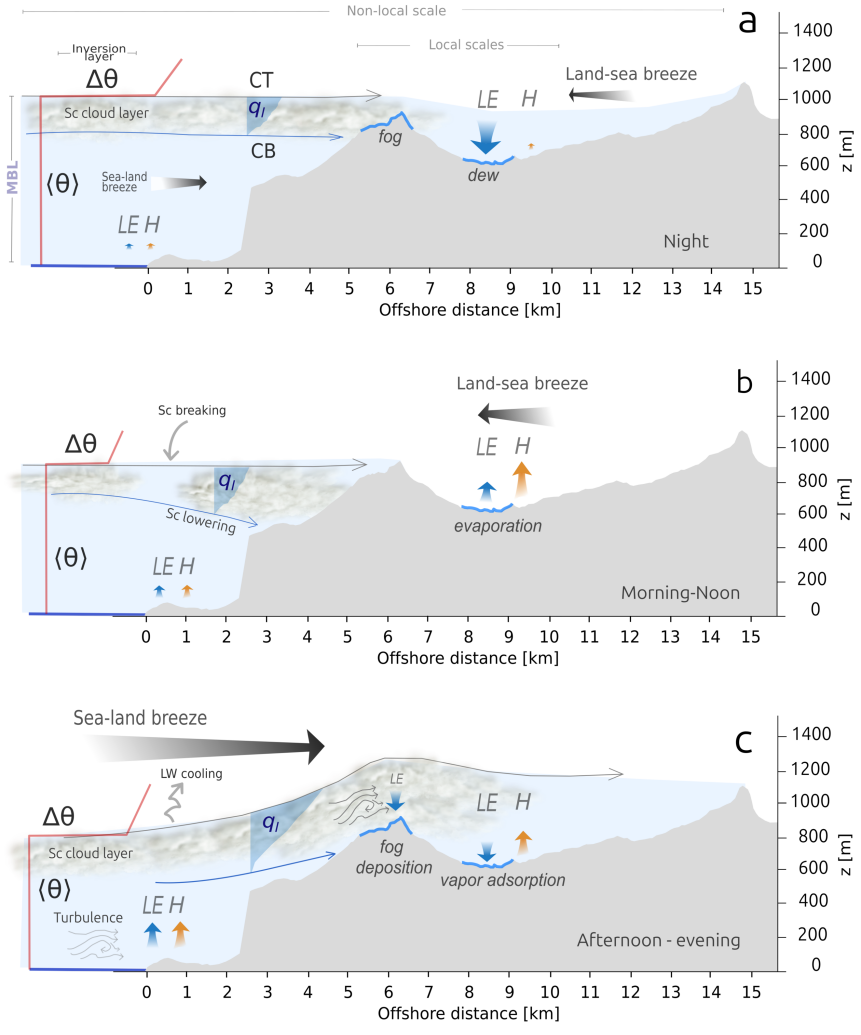

Figure 10. Schematic vertical cross-section of the dynamic of the MBL advection and the associated surface processes during (a) night, (b) morning-noon, (c) and afternoon-evening. $<\theta>$represents potential temperature, $\Delta\theta$ thermal inversion, q_l adiabatic liquid water content, LE latent heat flux, H sensible heat flux, and LW longwave.

LE values measured by eddy covariance flux towers have been used to interpret water vapor adsorption, fog, and dewfall in semi-arid savannas of Spain (Paulus et al., 2024). In this study system, the negative LE values between 0 and -100 W m^{-2} under non-saturated air conditions (RH ~70%) and T_s-T_{dew} > 0 °C reported are comparable to the conditions we observe at

https://doi.org/10.5194/egusphere-2026-2396
Preprint. Discussion started: 20 May 2026

the surface during the afternoon in our experiment, when water vapor adsorption occurs.

5 Conclusions

We study the processes triggered at the non-local (vertical) and local (near-surface and surface) scales when the marine Sc cloud-topped MBL is advected into hyperarid coastal topography in the Atacama Desert. By performing a field experiment, we analyzed in detail the temporal and spatial thermodynamic changes of the MBL and its water-energy exchange with the hyperarid surface. The experiment was designed to measure simultaneously vertical profiles of temperature, humidity, and wind speed along a topographic transect from 2 km offshore to 15 km inland. These vertical measurements were complemented by local observations of fog collection, routine meteorological variables, and surface fluxes along the transect.

Our field experiment allows us to conclude that the transition zone where Sc cloud turns into fog is a complex region marked by strong diurnal variability, resulting from the interaction of processes spanning synoptic (Sc cloud deck formation) to local (fog, dew, and water vapor adsorption) scales. Amid this strong diurnal variability, we identify three main regimes: fog maintenance (night), fog dissipation (morning), and fog advection (afternoon).

During the night, fog persists in the coastal mountains because land cools down, resulting in a thin but persistent cloud layer in contact with the windward mountain slopes. This thin cloud remains in a relatively steady state because weak marine winds are balanced with land-to-sea nocturnal katabatic winds, that blow in the opposite direction. This marine air maintains saturation as the saturated vapor pressure decreases and approaches actual vapor pressure under low temperature and humidity conditions, resulting in a cloud with low liquid water content and, therefore, low fog collection rates. At the same time, the unsaturated marine air trapped in more inland locations produces strong thermal contrasts with the surface, leading to a negative latent heat flux and dew formation. From the sunrise onwards, surface temperature triggers sensible and latent heat fluxes in the desert, dissipating clouds and evaporating the accumulated nocturnal dewfall. As temperature increases, the MBL thermal inversion decreases, producing cloud breaks that enhance fog dissipation. Likewise, the land-to-sea breeze dominates the sea-to-land breeze, transporting dry air from inland and contributing to fog dissipation.

In the afternoon, the thermal differences between the inland desert (warm) and the local ocean (cool) drive a sea-to-land breeze, which in turn initiates several processes along the interaction zone. First, nearshore wind shear generates mechanical turbulence, elevating surface sensible and latent heat fluxes below the MBL. However, since the Sc cloud shades this surface, the increase is not significant. Second, humidity advection from the ocean reaches its maximum, triggering the formation of a thicker Sc-fog cloud, which is then forced to lift by the steep topography. The (over)saturation of this marine air at the windward mountain slope has a higher liquid water content than in the morning, since the vapor pressure increases to reach saturated vapor pressure, yielding higher fog water collection. Finally, at the leeward mountain slope, marine unsaturated air advection transports humid air into recently desiccated surfaces, triggering rapid water vapor adsorption (negative latent heat flux). In the evening, fog dominates the windward and leeward slopes, producing surface fog deposition. The retention of oceanic humid air in the facing-ocean mountains of the coastal Atacama Desert dries the MBL as it moves inland, while potential temperature

https://doi.org/10.5194/egusphere-2026-2396
Preprint. Discussion started: 20 May 2026

remains steady.

This study was purely observational, and we describe how the MBL is affected by the hyperarid surface when the stratocumulus transitions to land fog. To better connect the processes involved and their meso and synoptic scales, in further studies, we plan to combine the StraToFog data with a modelling approach to analyse, quantify and represent the physical mechanisms described during the campaign.

Data availability. *StraToFog* data is available from the corresponding author upon reasonable request

Author contributions. The article was written by FL-R (lead) with contributions of OH, VE, KK, FM and FS. Measurements were taken by all authors. The experiment design was developed by OH and FL-R. The data were analyzed and visualized by FL-R. All the authors contributed to the revision of the manuscript

Competing interests. The authors declare that they have no conflict of interest

Acknowledgements. This research was funded by the Chilean National Commission of Science and Technology through ANID/FONDECYT/11250466 and ANID/ ATE/230006. A special acknowledgment to dr. Camilo del Rio for his help through the funding FONDEF IDeA ID23I10235 and dr. Ricardo Muñoz for fundamental fieldwork equipment provided. Finally, we acknowledge all students and researchers who participated during the campaign: Jorge Herrera, Amanda Peña-Echeverría, Javiera Boada-Campos, Catalina Arce, Jorge Renaud, Francisca Virtuoso, Catalina Contreras, Milton Avilés, and Margaret Shanafield.

https://doi.org/10.5194/egusphere-2026-2396
Preprint. Discussion started: 20 May 2026

References

Albornoz, F., del Río, C., Carter, V., Escobar, R., and Vásquez, L.: Fog water collection for local greenhouse vegetable production in the Atacama Desert, Sustainability, 15, 15 720, 2023.

Cereceda, P., Larrain, H., Osses, P., Lázaro, P., García, J., and Hernández, V.: El factor clima en la floración del desierto en los años "El Niño" 1991 y 1997, Revista de Geografía Norte Grande, pp. 37–52, 2000.

Cereceda, P., Osses, P., Larrain, H., Farıas, M., Lagos, M., Pinto, R., and Schemenauer, R.: Advective, orographic and radiation fog in the Tarapacá region, Chile, Atmospheric Research, 64, 261–271, 2002.

Cereceda, P., Larrain, H., Osses, P., Farias, M., and Egaña, I.: The spatial and temporal variability of fog and its relation to fog oases in the Atacama Desert, Chile, Atmospheric Research, 87, 312–323, 2008.

del Río, C., Garcia, J.-L., Osses, P., Zanetta, N., Lambert, F., Rivera, D., Siegmund, A., Wolf, N., Cereceda, P., Larraín, H., et al.: ENSO influence on coastal fog-water yield in the Atacama Desert, Chile, Aerosol and Air Quality Research, 18, 127–144, 2018.

Del Río, C., Lobos, F., Siegmund, A., Tejos, C., Osses, P., Huaman, Z., Meneses, J. P., and García, J.-L.: GOFOS, ground optical fog observation system for monitoring the vertical stratocumulus-fog cloud distribution in the coast of the Atacama Desert, Chile, Journal of Hydrology, 597, 126 190, 2021.

Duynkerke, P., Zhang, H., and Jonker, P.: Microphysical and turbulent structure of nocturnal stratocumulus as observed during ASTEX, Oceanographic Literature Review, 3, 229, 1996.

Espinoza, V., Lobos-Roco, F., and del Río, C.: Synoptic control of the spatiotemporal variability of fog and low clouds under ENSO phenomena along the Chilean coast (17-36 S), Atmospheric Research, 308, 107 533, 2024.

García, J.-L., Lobos-Roco, F., Schween, J. H., del Río, C., Osses, P., Vives, R., Pezoa, M., Siegmund, A., Latorre, C., Alfaro, F., et al.: Climate and coastal low-cloud dynamic in the hyperarid Atacama fog Desert and the geographic distribution of Tillandsia landbeckii (Bromeliaceae) dune ecosystems, Plant Systematics and Evolution, 307, 57, 2021.

Heusinkveld, B. G., Berkowicz, S. M., Jacobs, A. F., Holtslag, A. A., and Hillen, W. C.: An automated microlysimeter to study dew formation and evaporation in arid and semiarid regions, Journal of Hydrometeorology, 7, 825–832, 2006.

Houston, J.: Variability of precipitation in the Atacama Desert: its causes and hydrological impact, International Journal of Climatology: A Journal of the Royal Meteorological Society, 26, 2181–2198, 2006.

Jacobs, A. F., Heusinkveld, B. G., and Berkowicz, S. M.: Dew deposition and drying in a desert system: a simple simulation model, Journal of Arid Environments, 42, 211–222, 1999.

Jacobs, A. F., Heusinkveld, B. G., Wichink Kruit, R. J., and Berkowicz, S. M.: Contribution of dew to the water budget of a grassland area in the Netherlands, Water Resources Research, 42, 2006.

Keim-Vera, K., Lobos-Roco, F., Aguirre, I., Merino, C., and Del Río, C.: Fog types frequency and their collectable water potential in the Atacama Desert, Atmospheric Research, 312, 107 747, 2024.

Larrain, H., Velásquez, F., Cereceda, P., Espejo, R., Pinto, R., Osses, P., and Schemenauer, R.: Fog measurements at the site "Falda Verde" north of Chañaral compared with other fog stations of Chile, Atmospheric Research, 64, 273–284, 2002.

Lehnert, L. W., Thies, B., Trachte, K., Achilles, S., Osses, P., Baumann, K., Schmidt, J., Samolov, E., Jung, P., Leinweber, P., et al.: A case study on fog/low stratus occurrence at Las Lomitas, Atacama Desert (Chile) as a water source for biological soil crusts, Aerosol and Air Quality Research, 18, 254–269, 2018.

https://doi.org/10.5194/egusphere-2026-2396
Preprint. Discussion started: 20 May 2026

Lobos-Roco, F., de Arellano, J. V.-G., and Pedruzo-Bagazgoitia, X.: Characterizing the influence of the marine stratocumulus cloud on the land fog at the Atacama Desert, Atmospheric research, 214, 109–120, 2018.

Lobos-Roco, F., Hartogensis, O., Vilà-Guerau de Arellano, J., De La Fuente, A., Muñoz, R., Rutllant, J., and Suárez, F.: Local evaporation controlled by regional atmospheric circulation in the Altiplano of the Atacama Desert, Atmospheric Chemistry and Physics, 21, 9125–9150, 2021.

Lobos-Roco, F., Suárez, F., Aguirre-Correa, F., Keim, K., Aguirre, I., Vargas, C., Abarca, F., Ramírez, C., Escobar, R., Osses, P., et al.: Understanding inland fog and dew dynamics for assessing potential non-rainfall water use in the Atacama, Journal of Arid Environments, 221, 105 125, 2024.

Lobos-Roco, F., Vilà-Guerau de Arellano, J., and del Río, C.: Observation-driven model for calculating water-harvesting potential from advective fog in (semi-) arid coastal regions, Hydrology and Earth System Sciences, 29, 109–125, 2025.

Malik, D., Andersen, H., Cermak, J., Vogt, R., and Adler, B.: Cloud base height determines fog occurrence patterns in the Namib Desert, Atmospheric Chemistry and Physics, 26, 681–701, 2026.

Montecinos, S., Carvajal, D., Cereceda, P., and Concha, M.: Collection efficiency of fog events, Atmospheric research, 209, 163–169, 2018.

Muñoz, R. C., Falvey, M. J., Araya, M., and Jacques-Coper, M.: Strong down-valley low-level jets over the Atacama Desert: Observational characterization, Journal of applied meteorology and climatology, 52, 2735–2752, 2013.

Muñoz-Schick, M., Pinto, R., Mesa, A., and Moreira-Muñoz, A.: " Oasis de neblina" en los cerros costeros del sur de Iquique, región de Tarapacá, Chile, durante el evento El Niño 1997-1998, Revista chilena de historia natural, 74, 389–405, 2001.

Paulus, S. J., Orth, R., Lee, S.-C., Hildebrandt, A., Jung, M., Nelson, J. A., El-Madany, T. S., Carrara, A., Moreno, G., Mauder, M., et al.: Interpretability of negative latent heat fluxes from eddy covariance measurements in dry conditions, Biogeosciences, 21, 2051–2085, 2024.

Pinto, R., Barría, I., and Marquet, P. A.: Geographical distribution of Tillandsia lomas in the Atacama Desert, northern Chile, Journal of arid environments, 65, 543–552, 2006.

Rahn, D. and Garreaud, R.: Marine boundary layer over the subtropical southeast Pacific during VOCALS-REx–Part 1: Mean structure and diurnal cycle, Atmospheric Chemistry and Physics, 10, 4491–4506, 2010.

Rutllant, J., Muñoz, R., and Garreaud, R.: Meteorological observations on the northern Chilean coast during VOCALS-REx, Atmospheric Chemistry and Physics, 13, 3409–3422, 2013.

Rutllant, J. A., Fuenzalida, H., and Aceituno, P.: Climate dynamics along the arid northern coast of Chile: The 1997–1998 Dinámica del Clima de la Región de Antofagasta (DICLIMA) experiment, Journal of Geophysical Research: Atmospheres, 108, 2003.

Schemenauer, R. S. and Cereceda, P.: A proposed standard fog collector for use in high-elevation regions, Journal of applied Meteorology and Climatology, 33, 1313–1322, 1994.

Schween, J. H., del Rio, C., García, J.-L., Osses, P., Westbrook, S., and Löhnert, U.: Life cycle of stratocumulus clouds over one year at the Coast of the Atacama Desert, Atmospheric Chemistry and Physics Discussions, 2022, 1–33, 2022.

Thiel, M., Castilla, J. C., Fernández, M., and Navarrete, S.: The Humboldt current system of northern and central Chile, 2007.

Wetzel, P. J.: A simple parcel method for prediction of cumulus onset and area-averaged cloud amount over heterogeneous land surfaces, Journal of Applied Meteorology and Climatology, 29, 516–523, 1990.

Wood, R.: Stratocumulus clouds, Monthly Weather Review, 140, 2373–2423, 2012.